AMERICAN SOCIETY FOR MICROBIOLOGY | Journal of Bacteriology®

RESEARCH ARTICLE

The *Pseudomonas aeruginosa* PrrF1 and PrrF2 Small Regulatory RNAs Promote 2-Alkyl-4-Quinolone Production through Redundant Regulation of the *antR* mRNA

Louise Djapgne,[a] Subrata Panja,[b] Luke K. Brewer,[a] Jonathan H. Gans,[a] Maureen A. Kane,[a] Sarah A. Woodson,[b] Amanda G. Oglesby-Sherrouse[a,c]

[a]University of Maryland School of Pharmacy, Department of Pharmaceutical Sciences, Baltimore, Maryland, USA

[b]Johns Hopkins University, Krieger School of Arts and Sciences, Department of Biophysics, Baltimore, Maryland, USA

[c]University of Maryland, School of Medicine, Department of Microbiology and Immunology, Baltimore, Maryland, USA

ABSTRACT *Pseudomonas aeruginosa* is an opportunistic Gram-negative pathogen that requires iron for growth and virulence. Under low-iron conditions, *P. aeruginosa* transcribes two highly identical (95%) small regulatory RNAs (sRNAs), PrrF1 and PrrF2, which are required for virulence in acute murine lung infection models. The PrrF sRNAs promote the production of 2-akyl-4(1*H*)-quinolone metabolites (AQs) that mediate a range of biological activities, including quorum sensing and polymicrobial interactions. Here, we show that the PrrF1 and PrrF2 sRNAs promote AQ production by redundantly inhibiting translation of *antR*, which encodes a transcriptional activator of the anthranilate degradation genes. A combination of genetic and biophysical analyses was used to define the sequence requirements for PrrF regulation of *antR*, demonstrating that the PrrF sRNAs interact with the *antR* 5′ untranslated region (UTR) at sequences overlapping the translational start site of this mRNA. The *P. aeruginosa* Hfq protein interacted with UA-rich sequences in both PrrF sRNAs (K_d [dissociation constant] = 50 nM and 70 nM). Hfq bound with lower affinity to the *antR* mRNA (0.3 μM), and PrrF was able to bind to *antR* mRNA in the absence of Hfq. Nevertheless, Hfq increased the rate of PrrF annealing to the *antR* UTR by 10-fold. These studies provide a mechanistic description of how the PrrF1 and PrrF2 sRNAs mediate virulence traits, such as AQ production, in *P. aeruginosa*.

IMPORTANCE The iron-responsive PrrF sRNAs play a central role in regulating *P. aeruginosa* iron homeostasis and pathogenesis, yet the molecular mechanisms by which PrrF regulates gene expression are largely unknown. In this study, we used genetic and biophysical analyses to define the interactions of the PrrF sRNAs with Hfq, an RNA annealer, and the *antR* mRNA, which has downstream effects on quorum sensing and virulence factor production. These studies provide a comprehensive mechanistic analysis of how the PrrF sRNAs regulate virulence trait production through a key mRNA target in *P. aeruginosa*.

KEYWORDS *Pseudomonas aeruginosa*, PrrF, PQS, Hfq, iron, *ant*R

Pseudomonas aeruginosa is a Gram-negative opportunistic pathogen that causes life-threatening infections in diverse patient populations. *P. aeruginosa* virulence depends on a multitude of virulence factors that include exotoxins (1–3), cell-to-cell communication via quorum-sensing factors (4–6), and nutrient acquisition systems (7). Nutrients, such as iron, are sequestered from invading pathogens by the innate immune system through a process referred to as nutritional immunity (8). Iron is critical for maintaining *P. aeruginosa* growth and virulence, and *P. aeruginosa* uses multiple

Received 20 November 2017 **Accepted** 1 March 2018

Accepted manuscript posted online 5 March 2018

Citation Djapgne L, Panja S, Brewer LK, Gans JH, Kane MA, Woodson SA, Oglesby-Sherrouse AG. 2018. The *Pseudomonas aeruginosa* PrrF1 and PrrF2 small regulatory RNAs promote 2-alkyl-4-quinolone production through redundant regulation of the *antR* mRNA. J Bacteriol 200: e00704-17. https://doi.org/10.1128/JB.00704-17.

Editor George O'Toole, Geisel School of Medicine at Dartmouth

Address correspondence to Sarah A. Woodson, swoodson@jhu.edu, or Amanda G. Oglesby-Sherrouse, aoglesby@rx.umaryland.edu.

pathways to acquire the metal from its host, including siderophore-dependent systems, heme acquisition pathways, and ferrous iron transporters (7, 9–11). In order to limit uptake of this redox-active metal, *P. aeruginosa* also possesses an intricate regulatory cascade that regulates the expression of iron uptake systems in response to available iron sources (12). This system is largely presided over by the ferric uptake regulator (Fur) protein, an iron-binding transcriptional repressor that blocks the expression of *P. aeruginosa*'s iron uptake regulon under iron-replete conditions. The Fur protein also regulates the expression of numerous virulence factors, including secreted proteases and exotoxin A (13–17). This response allows *P. aeruginosa* to deploy its arsenal of virulence factors upon host-employed iron starvation, highlighting iron as a major environmental regulator of pathogenesis.

P. aeruginosa virulence and iron homeostasis also depend on the Fur-regulated PrrF1 and PrrF2 sibling small regulatory RNAs (sRNAs) (18, 19). The PrrF1 and PrrF2 sRNAs are 95% identical to one another, and they are transcribed from genes that are located in tandem on the genome in all sequenced strains of *P. aeruginosa* (20). The PrrF sRNAs are transcribed in response to iron depletion and contribute to iron homeostasis by blocking the production of nonessential iron-containing proteins (21). The PrrF sRNAs have also been shown to promote the production of several 2-alkyl-4(1*H*)-quinolone metabolites (AQs) (14, 18), which mediate a variety of biological activities that are important for virulence. These AQs include the *Pseudomonas* quinolone signal (PQS) and 2-heptyl-4-hydroxyquinolone (HHQ) quorum-sensing molecules, which induce the expression of multiple virulence genes (22–24). The AQ-biosynthetic pathway also produces an *N*-oxide-substituted AQ, 2-heptyl-4-hydroxyquinolone *N*-oxide (HQNO). HQNO promotes virulence by exerting toxic effects on mammalian cells and may also limit the growth of competing microbial species during polymicrobial infections (25–27). The PrrF sRNAs increase the production of each of these AQs, indicating their effects occur at the initiation of AQ synthesis (18). PrrF is thought to promote AQ synthesis by blocking the expression of the *antABC* and *catBCA* genes, which encode enzyme complexes that mediate degradation of the AQ precursor, anthranilate (Fig. 1A). Supplementation of Δ*prrF1,2* mutant cultures with anthranilate restores production of PQS (14), supporting the model in which PrrF regulation of anthranilate metabolism underlies the requirement for PrrF in AQ biosynthesis (28).

Bacterial sRNAs typically function by complementary base pairing with mRNA molecules, which can lead to either positive or negative effects on mRNA stability and expression (29–32). Base pairing of the sRNA near the ribosomal binding site (RBS) of the mRNA most often results in decreased mRNA stability and reduced translation efficiency. In contrast, base pairing of the sRNA upstream of the translational start site has been shown to alter the secondary structure of some mRNAs, resulting in increased translation efficiency. Both the PrrF1 and PrrF2 sRNAs share significant complementarity with the RBS and surrounding region of the *antR* mRNA (Fig. 1B), encoding a LysR-type transcriptional activator of the *antABC* and *catBCA* operons (14). A recent study demonstrated that overexpression of the PrrF2 sRNA resulted in decreased translation of the *antR* mRNA in *P. aeruginosa* (33). The authors of the study further showed that this regulation depended on the *P. aeruginosa* Hfq RNA binding protein, which we previously found interacts with the PrrF sRNAs (34). This finding is in line with what has been shown for the Hfq proteins of many other bacterial species, including *Escherichia coli*, where the Hfq protein accelerates annealing of sRNAs with their target mRNA molecules (33, 35–39). However, neither the biophysical basis of this regulation nor its impact on PrrF-regulated AQ production has been determined.

In the current study, we sought to determine the mechanisms underlying PrrF regulation of AQ production. We show that the PrrF1 and PrrF2 sRNAs function redundantly to repress *antR* expression and promote AQ production. We further show that this regulation occurs through posttranscriptional regulation by the PrrF sRNAs via the 5′ untranslated region (UTR) of the *antR* mRNA. We mapped the nucleotides required for interaction of the PrrF sRNAs with the *antR* mRNA through a combination of *in vivo* and *in vitro* analyses. We further showed that the *P. aeruginosa* Hfq protein

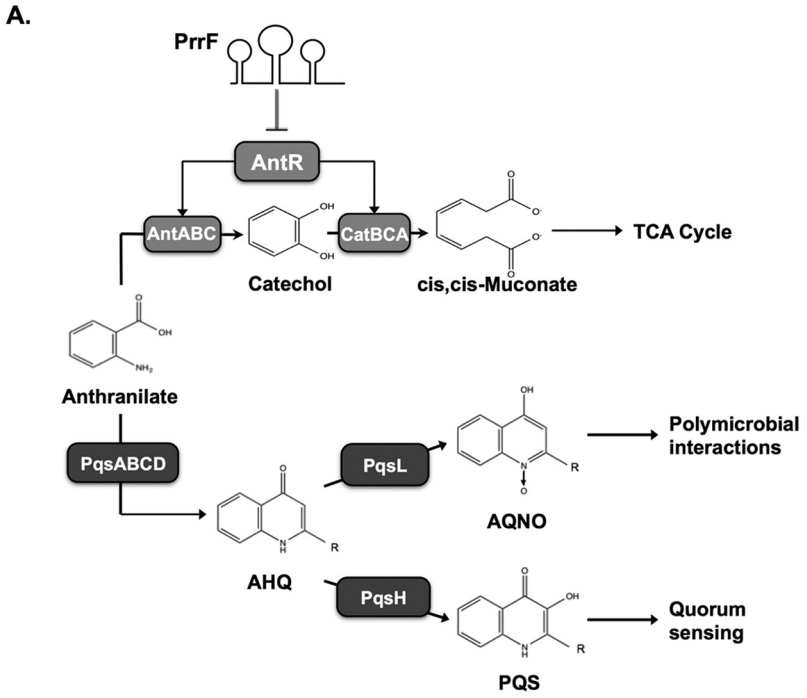

B.

```
PrrF1: 96 ACGGCCCAGUUUUUGGCACUAAUCGGACUACUCCU 60
          ||||| ||| |: :|||     | | |||||||||
antR: -21 UGCCGUGUCGAGUGCCGA----ACCAUGAUGAGGA 10
                      ****    *********

PrrF2: 95 ACGGCCCAG-CUUUGGCACUAAUCGGACUACUCCU 60
          ||||| |||  : :|||     | | |||||||||
antR: -21 UGCCGUGUCGAGUGCCGA----ACCAUGAUGAGGA 10
```

FIG 1 Model of PrrF-regulated production of 2-alkyl-4-quinolones. (A) PrrF sRNAs are predicted to promote alkylquinolone production by regulating the metabolism of anthranilate. In this model, the PrrF sRNAs repress the expression of *antR*, encoding a LysR-type transcriptional activator that induces expression of *antABC*, and *catBCA* genes for anthranilate catabolism. This prevents the degradation of anthranilate, allowing the metabolite to instead be used for the synthesis of numerous 2-akyl-4(1*H*)-quinolone metabolites via the *pqsABCDE*, *pqsH*, and *pqsL* gene products, as previously described. R indicates the presence of an alkyl chain, which varies in length and saturation. (B) Predicted complementarity between the PrrF1 and PrrF2 sRNAs and the *antR* leader sequence. The numbers indicate the orientation in relation to the transcriptional start site (PrrF1 and PrrF2) or the translational start site (*antR* leader). The predicted start codon of the *antR* mRNA is underlined. The asterisks indicate the region of *antR* that was protected by PrrF1 in RNase protection analysis performed in the present study. Vertical lines indicate canonical base pairing. Colons indicate noncanonical (G-U) base pairing. Dashes indicate gaps in the base pairing.

binds tightly to the PrrF sRNAs and increases their rate of annealing to the *antR* mRNA leader sequence. These data provide a comprehensive model based on genetic, biophysical, and metabolite analyses for how the iron-responsive PrrF sRNAs promote the production of AQs by *P. aeruginosa*.

RESULTS

Anthranilate supplementation restores production of most alkylquinolones to the Δ*prrF1,2* mutant. Previous studies using thin-layer chromatography (TLC) showed that anthranilate supplementation restored PQS production to the Δ*prrF1,2* mutant (14). This led to the model (Fig. 1A) in which PrrF repression of the *antABC* and *catBCA* genes spared anthranilate from degradation so that it could be used to synthesize PQS. If this is the case, then anthranilate supplementation should also restore production of other AQs, as anthranilate is a precursor for all of these metabolites. However, TLC does not detect the production of other AQ metabolites. We therefore determined the effect of anthranilate supplementation on AQ production, using a liquid chromatography-

TABLE 1 Anthranilate supplementation restores AQ production to the Δ*prrF1,2* mutant

Strain	Normalized concn [(μg/μl)/OD_{600}][a]					
	C_7-PQS	C_9-PQS	HHQ	NHQ	HQNO	NQNO
Wild type	0.37 ± 0.03	0.52 ± 0.03	0.10 ± 0.04	0.25 ± 0.09	1.56 ± 0.05	6.59 ± 0.34
Δ*prrF1,2* mutant	0.33 ± 0.03	0.27 ± 0.05[d]	0.04 ± 0.01[b]	0.11 ± 0.02[b]	0.83 ± 0.21[d]	3.73 ± 0.84[d]
Δ*prrF1,2* mutant + anthranilate	0.53 ± 0.03[d,f]	0.17 ± 0.02[d,e]	0.40 ± 0.09[c,f]	0.37 ± 0.05[b,f]	2.93 ± 0.31[d,f]	6.07 ± 0.76[e]

[a]The concentration of each AQ in the supernatants of the indicated strains grown in DTSB, with or without 500 μM anthranilate, as indicated, was determined by LC–MS-MS and normalized by culture density, as described in Materials and Methods. Significant differences were determined by two-tailed Student's *t* test. OD_{600}, optical density at 600 nm.

[b]$P < 0.05$ for the Δ*prrF1,2* mutant, with or without anthranilate, compared to the wild-type strain.

[c]$P < 0.005$ for the Δ*prrF1,2* mutant, with or without anthranilate, compared to the wild-type strain.

[d]$P < 0.0005$ for the Δ*prrF1,2* mutant, with or without anthranilate, compared to the wild-type strain.

[e]$P < 0.005$ for the Δ*prrF1,2* mutant with versus without anthranilate.

[f]$P < 0.0005$ for the Δ*prrF1,2* mutant with versus without anthranilate.

tandem mass spectrometry (LC–MS-MS) protocol previously developed in our laboratory (40, 41). The wild-type (WT) and Δ*prrF1,2* mutant strains were grown for 18 h in dialyzed tryptic soy broth (DTSB), an iron-depleted medium used extensively by our laboratory to analyze *P. aeruginosa* AQ production (14, 18, 40–42). This assay quantifies the levels of both the C_7 and C_9 congeners of the PQS, HHQ, and HQNO metabolites, which represent the most abundant congeners under a variety of culture conditions (43). As previously observed, the Δ*prrF1,2* mutant showed a significant reduction in the production of almost all the AQs tested by LC–MS-MS (Table 1). The one exception was the C_7 congener of PQS (C_7-PQS), which showed only a small and insignificant reduction in the Δ*prrF1,2* mutant (Table 1). With the exception of the C_9-PQS congener, supplementation of the Δ*prrF1,2* mutant cultures with 500 μM anthranilate restored production of AQs to levels at or above those of the wild-type strain (Table 1). Interestingly, anthranilate supplementation of Δ*prrF1,2* mutant cultures did not restore C_7-PQS and C_9-PQS production as robustly as previously observed by TLC (14). There was no significant difference in the concentration of individual AQ species produced by the Δ*prrF1* and Δ*prrF2* strains, indicating redundant effects of PrrF1 and PrrF2 sRNAs in regulating AQ production. This may be due to the production of multiple PQS congeners, with varying alkyl chain lengths and levels of saturation, that cannot be differentiated by TLC. Regardless, these data indicate that the Δ*prrF1,2* mutant defect in AQ production is due, at least in part, to deregulated anthranilate metabolism.

The PrrF sRNAs posttranscriptionally regulate expression of *antR*. We next investigated the genetic mechanism by which the PrrF sRNAs affect AQ production by analyzing expression of *antR*, which encodes a LysR-type transcriptional activator of the *antABC* and *catBCA* genes for anthranilate degradation. We first identified the *antR* transcriptional start site (TSS) by 5′ rapid amplification of cDNA ends (RACE) using RNA isolated from the wild-type PAO1 strain grown in DTSB with 100 μM $FeCl_3$ supplementation. This growth condition was previously shown to allow high levels of *antR* mRNA in PAO1 (14). The TSS was located within a string of G residues adjacent to sequence 95 to 98 nucleotides (nt) upstream of the translational start site (see Fig. S1 in the supplemental material). This TSS was distinct from that previously identified for *antR*, potentially due to the high-iron growth conditions used for the analysis, which produce a much higher level of *antR* transcription than was seen in the earlier study (44).

We next cloned the sequence corresponding to the predicted iron-dependent *antR* promoter, the *antR* untranslated region (UTR), and the portion of the *antR* coding sequence that is predicted to pair with the PrrF sRNAs and fused this fragment to a promoterless *lacZY* operon that lacked its native Shine-Dalgarno sequence (Fig. 2A). The resulting fusions were integrated onto the PAO1 and Δ*prrF1,2* chromosomes at the *att* site. The *antR* reporter strains were grown in DTSB, with or without supplementation with 100 μM $FeCl_3$, for 18 h. As expected, β-galactosidase activity was strongly repressed when the wild-type strain was grown under low-iron conditions. Also as expected, we observed significant induction of β-galactosidase activity in the Δ*prrF1,2* mutant reporter strain compared to the wild-type reporter strain when both were

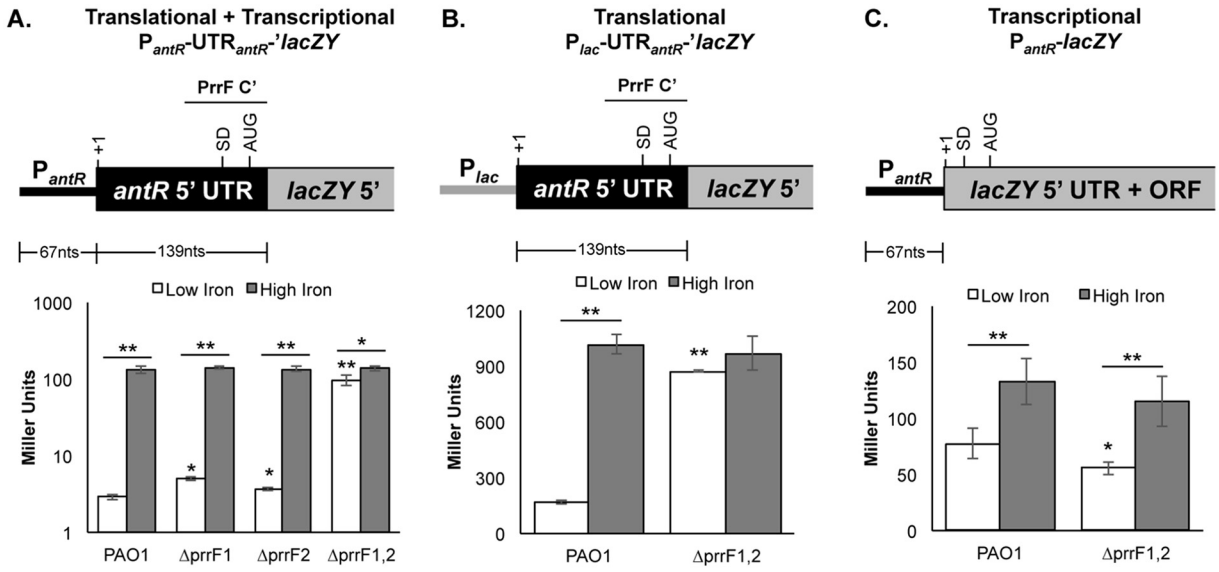

FIG 2 The PrrF sRNAs mediate iron-regulated posttranscriptional repression of *antR*. The indicated strains carrying the *antR* transcriptional and translational fusions (A), the *antR* translational fusion (B), or the *antR* transcriptional fusion (C) were grown for 18 h at 37°C in DTSB without (white bars) or with (gray bars) 100 μM $FeCl_3$ supplementation. Diagrams of the corresponding reporter fusions are shown above the graphs. In each diagram, +1 denotes the transcriptional start site, SD denotes the Shine-Dalgarno site, and AUG indicates the translational start site. In panels A and B, the region of PrrF complementarity (PrrF C′) with the *antR* UTR is indicated above the diagram by a horizontal bar. The error bars indicate the standard deviations of β-galactosidase activity from three (A) or six (B and C) independent experiments. The asterisks indicate a significant difference when comparing each of the mutants to PAO1 grown under low-iron conditions or as indicated by the horizontal bars. *, $P < 0.05$; **, $P < 0.001$.

grown in low iron (Fig. 2A). Interestingly, iron supplementation still caused a small but statistically significant induction of β-galactosidase activity from the *antR* reporter in the Δ*prrF1,2* mutant (Fig. 2A), indicating that iron activates *antR* expression through both PrrF-dependent and PrrF-independent pathways.

We next determined whether iron activation of *antR* expression occurs by transcriptional or posttranscriptional mechanisms. An *antR* translational fusion consisting of the native *lac* promoter followed by the *antR* 5′UTR fused to the *lacZY* operon, as shown in Fig. 2B, was integrated at the *att* site of PAO1 and the Δ*prrF1,2* mutant. The β-galactosidase activity from this translational reporter showed 7.3-fold induction by iron, and this induction was eliminated in the Δ*prrF1,2* mutant (Fig. 2B). We also constructed an *antR* transcriptional fusion consisting of the *antR* promoter fused to *lacZY* preceded by its native Shine-Dalgarno site (Fig. 2C). The *antR* transcriptional reporter was also activated by iron in wild-type PAO1, but only by 2.3-fold (Fig. 2C). Moreover, while a slight reduction in *antR* promoter activity was observed in the Δ*prrF1,2* mutant compared to the wild type, deletion of the *prrF1-prrF2* locus did not reduce iron activation of this reporter (Fig. 2C). Combined, these data demonstrate that PrrF-dependent iron activation of *antR* expression occurs via the *antR* 5′ UTR, while PrrF-independent iron activation of *antR* occurs at the *antR* promoter.

PrrF1 and PrrF2 promote AQ production through redundant repression of *antR* expression. Previous studies showed that the PrrF1 and PrrF2 sRNAs are redundant for regulation of many targets, including *antR* and *antA* (14, 21). However, the impact of the individual PrrF sRNAs on AQ production was not known. We therefore determined the impacts of the individual PrrF1 and PrrF2 sRNAs on AQ production by LC–MS-MS. The PAO1, Δ*prrF1*, and Δ*prrF2* single mutants and the Δ*prrF1,2* double mutant were grown in DTSB for 18 h and analyzed for AQ production by LC–MS-MS. Individual deletion of either the *prrF1* or *prrF2* gene exerted no effect on the production of C_7-PQS, HHQ, HQNO, or NQNO (2-nonyl-4-hydroxyquinoline n-oxide) (Table 2) and caused only small (less than 50%) reductions in C_9-PQS and NHQ production (Table 2). There was also no significant difference in the concentrations of individual AQ species produced

TABLE 2 PrrF1 and PrrF2 are redundant in their regulation of AQ production

Strain	Normalized concn [(μg/μl)/OD_{600}][a]					
	C_7-PQS	C_9-PQS	HHQ	NHQ	HQNO	NQNO
Wild type	0.64 ± 0.06	1.01 ± 0.10	0.08 ± 0.02	0.27 ± 0.07	2.39 ± 0.28	12.21 ± 1.03
Δ*prrF1* mutant	0.54 ± 0.08	0.65 ± 0.05[d]	0.05 ± 0.01	0.14 ± 0.03[b]	2.06 ± 0.62	9.82 ± 0.01
Δ*prrF2* mutant	0.55 ± 0.07	0.80 ± 0.06[c]	0.06 ± 0.01	0.17 ± 0.05	2.50 ± 0.61	11.10 ± 1.99
Δ*prrF1,2* mutant	0.50 ± 0.07[b]	0.35 ± 0.06[d]	0.04 ± 0.01[b]	0.06 ± 0.01[d]	0.95 ± 0.27[d]	3.71 ± 0.00[d]

[a]The concentration of each AQ in the supernatants of the indicated strains grown in DTSB was determined by LC–MS-MS and normalized by culture density, as described in Materials and Methods.
[b]$P < 0.05$, comparing the Δ*prrF1*, Δ*prrF2*, or Δ*prrF1,2* mutant to the wild type.
[c]$P < 0.005$, comparing the Δ*prrF1*, Δ*prrF2*, or Δ*prrF1,2* mutant to the wild type.
[d]$P < 0.0005$, comparing the Δ*prrF1*, Δ*prrF2*, or Δ*prrF1,2* mutant to the wild type.

by the Δ*prrF1* and Δ*prrF2* strains, indicating redundant effects of PrrF1 and PrrF2 sRNAs in regulating AQ production. The *antR* reporter fusion was also integrated onto the chromosomes of the Δ*prrF1* and Δ*prrF2* single mutants, and the resulting strains were grown for 18 h in DTSB and analyzed for β-galactosidase activity. Similar to what was observed for the production of most AQs, deletion of either *prrF1* or *prrF2* resulted in no significant change in β-galactosidase activity from the *antR* reporter (Fig. 2B). These data demonstrate that the PrrF1 and PrrF2 sRNAs redundantly regulate *antR* expression to promote AQ production.

PrrF represses *antR* via sequences in the *antR* UTR. We next sought to identify the specific nucleotides of the *antR* leader sequence that are required for regulation by the PrrF1 and PrrF2 sRNAs. A series of mutations were designed and introduced into the *antR* reporter (Fig. 3A), and the altered *antR* reporters were integrated at the *att* site of wild-type strain PAO1. While mutation of the sequence adjacent to the RBS ablated β-galactosidase activity from the *antR* reporter under high-iron conditions (alt-*antRA*

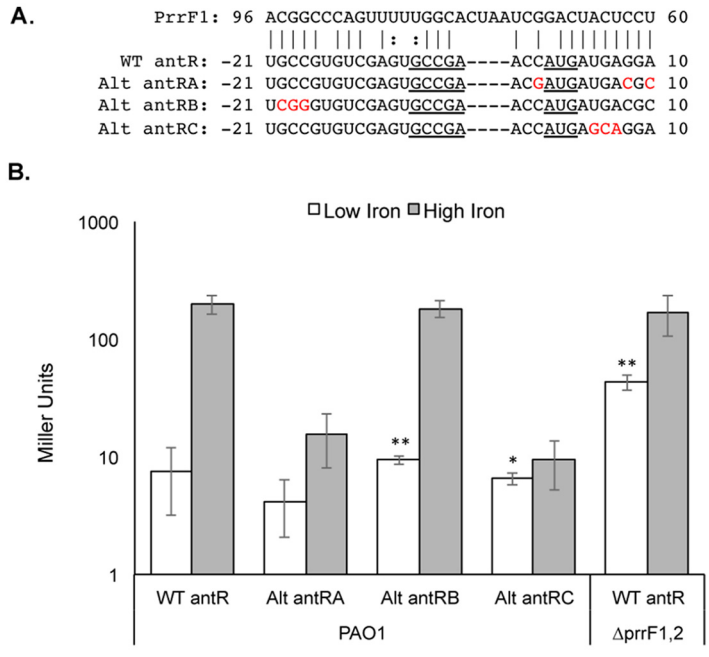

FIG 3 Mutations in the *antR* 5′ UTR reduce PrrF repression. (A) Mutations were generated in the *antR* translational fusion to disrupt the predicted interaction between the PrrF sRNAs and the *antR* 5′ UTR. (B) The indicated strains carrying either the WT or altered *antR* translational reporters shown in panel A were grown for 18 h in DTSB without (white bars) or with (gray bars) 100 μM $FeCl_3$ supplementation, and the cultures were assayed for β-galactosidase activity. The error bars represent the standard deviations from three independent experiments. The asterisks indicate a significant difference in Miller units when comparing the low-iron values to those of the WT *antR* translational reporter in strain PAO1 grown under low-iron conditions. *, $P < 0.01$; **, $P < 0.005$.

and alt-*antRC* mutants [Fig. 3B]), mutation of the sequence further upstream of the RBS had no significant effect on the β-galactosidase activity of the *antR* reporter under high-iron conditions (alt-*antRB* mutation [Fig. 3B]). We further explored the effects of the alt-*antRB* mutant, which altered 3 nucleotides approximately 20 nt upstream of the *antR* RBS, on β-galactosidase activity from the *antR* reporter under low-iron conditions. These data showed a small but statistically significant derepression of β-galactosidase activity from the alt-*antRB* reporter compared to the wild-type *antR* reporter when grown in iron-depleted medium (Fig. 3B). Despite showing reduced translation efficiency under high-iron conditions, the alt-*antRC* reporter also caused a small but statistically significant increase in β-galactosidase activity under low-iron conditions (Fig. 3B). Combined, these data suggest that PrrF repression of *antR* depends upon a significant stretch of complementarity between the PrrF sRNAs and the *antR* 5′ UTR. We attempted to restore PrrF regulation of the altered alt-*antRB* reporter by transforming the alt-*antRB* reporter strain with a plasmid carrying a compensatory *prrF1-prrF2* allele designed to restore PrrF1-*antR* and PrrF2-*antR* complementarity. However, this construct had no effect on β-galactosidase activity from the alt-*antRB* reporter, potentially due to altered structures of the PrrF or *antR* UTR (data not shown). Further analysis of the PrrF-*antR* interaction, including the role of the *P. aeruginosa* Hfq protein in their association, was therefore conducted *in vitro*.

PrrF sRNAs bind to the arginine patch of Hfq. The PrrF sRNAs were previously shown to interact with the *P. aeruginosa* Hfq protein (34), indicating a role for Hfq in PrrF regulatory function. Studies of *E. coli* and *Salmonella* sRNAs showed that the 3′-terminal U's associated with the Rho-independent transcription terminator bind the proximal pore of Hfq (45, 46). An internal AU-rich motif additionally interacts with the arginine patch on the rim of Hfq (47, 48), which is necessary for efficient annealing with its mRNA targets (36). To probe the secondary structure of the PrrF sRNAs and locate the *P. aeruginosa* Hfq binding site, we partially digested ^{32}P-labeled PrrF sRNAs with RNase If. The RNase If digestion pattern of PrrF1 in the absence of Hfq [Fig. 4A, lane (−) Hfq] agrees with the predicted secondary structure of PrrF1 (Fig. 4E), except that the regions between nt 60 and 65 and nt 80 and 90 were more protected than expected, suggesting that the region between stem-loop 2 and stem-loop 3 forms one or more alternative secondary structures.

The presence of *P. aeruginosa* Hfq weakly protected AU-rich segments of PrrF1, A58 to U59 and A69 to A72, and more strongly protected the U-rich motifs, U76 to A81 and U85 to U89, from digestion by RNase If (Fig. 4A, lanes *Pa* Hfq, and E, red symbols). The extent of protection increased with increasing Hfq concentrations, suggesting that these internal A/U- and U-rich motifs bind Hfq, as observed in other sRNAs. For comparison, we also probed the structure of PrrF1 RNA in the presence of *E. coli* Hfq, which also protected nt 76 to 89 of PrrF1, as we found with *P. aeruginosa* Hfq (Fig. 4A, *Ec* Hfq, lane 0.17 μM WT). Interestingly, when R16 on the rim of *E. coli* Hfq was replaced with alanine, this internal A/U-rich region was no longer protected from RNase digestion (Fig. 4A, *Ec* Hfq, lane 0.33 μM R16A), suggesting that this region interacts with the arginine patch. PrrF2 sRNA, which differs by only a few nucleotides from PrrF1, exhibited a similar RNase If digestion pattern in the absence and presence of *P. aeruginosa*, WT *E. coli*, and R16A Hfq (see Fig. S2 and S3 in the supplemental material). These results indicate that *P. aeruginosa* Hfq recognizes the PrrF1 and PrrF2 sRNAs in a manner similar to that of Hfq proteins from *E. coli* and *Salmonella*.

Hfq and PrrF1 bind different domains of the *antR* mRNA leader. To map the binding sites for *P. aeruginosa* Hfq and PrrF1 on the *antR* mRNA leader, a ^{32}P-labeled fragment of the *antR* mRNA from the transcription start site through the 14th codon was also partially digested with RNase If in the presence of *P. aeruginosa* Hfq and PrrF1. GC-rich sequences at the 5′ end of *antR* mRNA were completely protected from RNase digestion, consistent with the formation of stable secondary structure at the 5′ end of the mRNA (Fig. 4B). In the presence of Hfq, the A-rich loop between nt 42 and 50 of the *antR* mRNA was moderately protected from RNase digestion (Fig. 4B, lane A H and lane

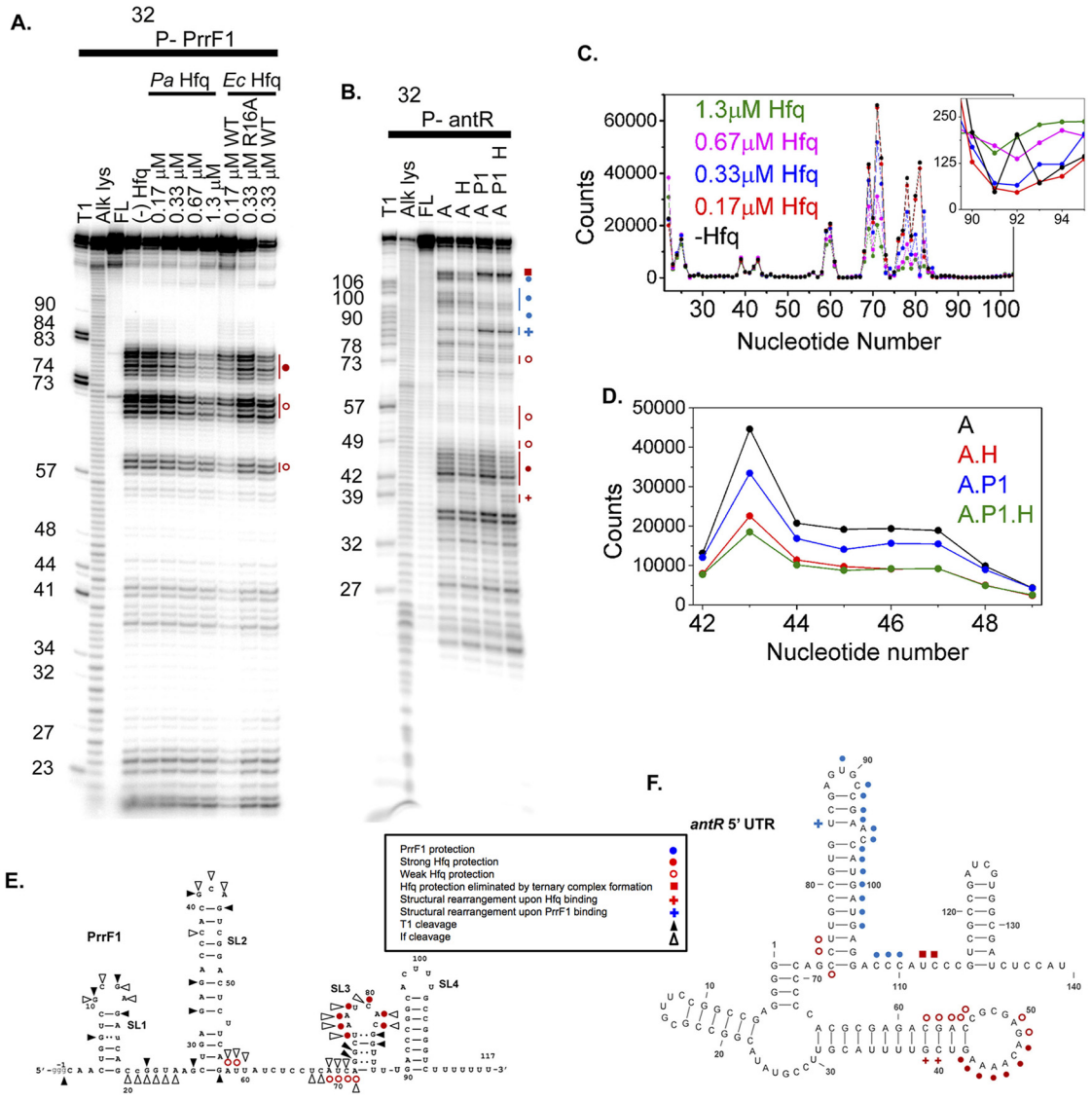

FIG 4 RNase If footprinting of PrrF1 and *antR*. (A) RNase If digestion pattern of 5′-^{32}P-PrrF1 sRNA at 30°C with no Hfq [(−) Hfq], 0.17 to 0.67 μM *P. aeruginosa* (*Pa*) Hfq, 0.17 to 0.33 μM *E. coli* (*Ec*) Hfq, and 0.33 μM *E. coli* R16A Hfq, as shown. Lanes T1, Alk lys, and FL represent control reactions in urea with RNase T1 (T1), alkaline hydrolysis (Alk lys), and no treatment (FL). *E. coli* Hfq binds sRNA more strongly than *P. aeruginosa* Hfq, and binding of a second *E. coli* Hfq hexamer may account for some differences between the protection pattern in 0.17 and 0.33 μM *E. coli* Hfq. (B) RNase If digestion patterns of 5′-^{32}P-labeled *antR* mRNA at 30°C with no Hfq (lane A), 0.5 μM *P. aeruginosa* Hfq (lane A H), 0.5 μM PrrF1 (lane A P1), and 0.5 μM *P. aeruginosa* Hfq plus 0.5 μM PrrF1 (lane A P1 H). Control reactions were as for panel A. Numbers to the left of the images in panels A and B indicate the nucleotide numbers of the RNA molecule where cleavage occurs to produce the observed bands. (C) Relative digestion of PrrF1 sRNA by RNase If in the absence and presence of *P. aeruginosa* Hfq (see Materials and Methods). The inset shows the region between nt 90 and 95. (D) Relative digestion of *antR* mRNA by RNase If in the absence and presence of *P. aeruginosa* Hfq and PrrF1 sRNA. (E and F) Summary of nuclease digestion patterns on the predicted secondary structures of PrrF1 (E) and *antR* 5′ UTR (F), as indicated in the key. The schematics summarize the results of several footprinting experiments for each RNA. Weak (<2×) and strong (~2×) protection were determined by quantitation of the footprinting gels with SAFA (71), as illustrated in panels C and D. A plus sign indicates increased nuclease cleavage upon Hfq (red) or PrrF1 (blue) binding, suggesting structural rearrangements of the RNA molecules. The secondary structures of the PrrF1 sRNA and *antR* mRNA shown in panels E and F, respectively, were generated using a combination of computational prediction (MFold) (73) and experimental results (A and B).

A H P1), suggesting this loop provides a weak binding site for Hfq in the *antR* mRNA (Fig. 4F, red circles). *P. aeruginosa* Hfq also protected residues downstream of the PrrF binding site (U112), but not when PrrF1 was present (Fig. 4F, red squares). When PrrF1 sRNA was allowed to bind *antR* mRNA, a downstream region spanning nt 91 to 110 became strongly protected from RNase If (Fig. 4C, lane A P and lane A H P1, and F, blue symbols). These residues comprise part of the predicted region of complementarity

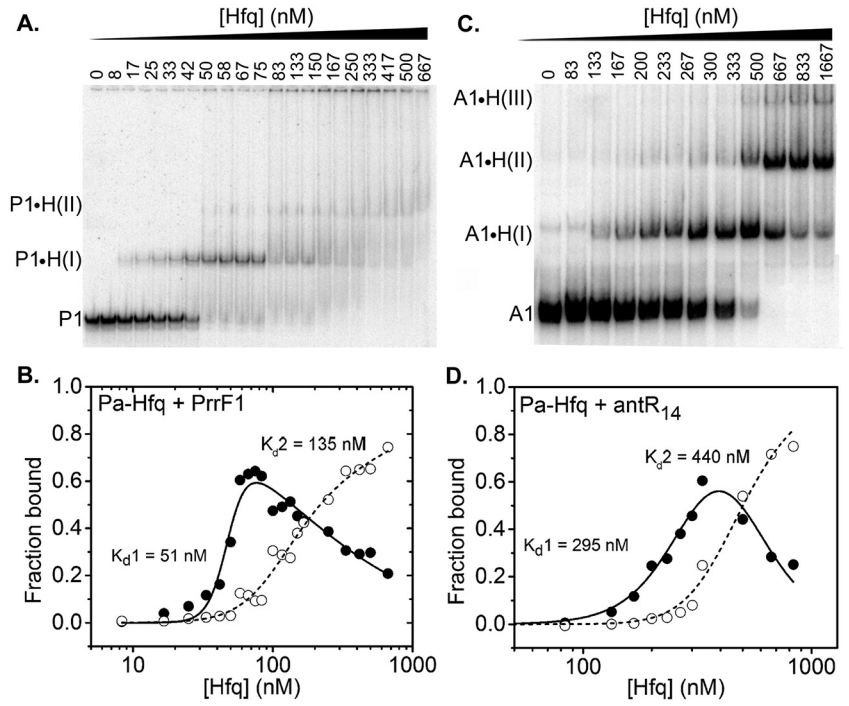

FIG 5 Equilibrium binding of Hfq with PrrF1 and *antR*. (A) Incubation of ^{32}P-labeled PrrF1 with 0 to 667 nM Hfq_6 resulted in a specific mobility shift [P1-H(I)], followed by an additional diffuse mobility shift [P1-H(II)] arising from two or more Hfq hexamers binding to PrrF1. (B) Fractions of P1-H(I) and P1-H(II) complexes were fit to equations 1 and 2 to obtain the dissociation constants (Table 3). (C) Titration of ^{32}P-*antR* mRNA with 0 to 1,667 nM Hfq_6 resulted in three distinct RNPs, A1-H(I), A1-H(II,) and A1-H(III), with one to three Hfq hexamers, respectively. (D) Fractions of A1-H(I) and the total of A1-H(II) plus A1-H(III) complexes, as in panel B.

between PrrF1 and *antR* mRNA (Fig. 3A) and coincide with the sequence required for full PrrF repression of P_{antR} translational activity *in vivo* (Fig. 3B, alt-*antRC*), indicating that this region is a likely binding site for PrrF1. The region was also protected when PrrF1 and *P. aeruginosa* Hfq were added to *antR* mRNA simultaneously, suggesting that PrrF1 can bind to *antR* mRNA in the absence or presence of *P. aeruginosa* Hfq.

***P. aeruginosa* Hfq binds to PrrF sRNA with higher affinity than to *antR* mRNA.** To determine whether *P. aeruginosa* Hfq can facilitate base pairing between sRNAs and mRNAs by simultaneously binding both RNAs in a ternary complex, we measured the affinity of *P. aeruginosa* Hfq for PrrF sRNAs and *antR* mRNA by native gel electrophoretic mobility shift assays (EMSA). When ^{32}P-labeled PrrF1 or PrrF2 was titrated with *P. aeruginosa* Hfq, we observed sequential gel shifts corresponding to the binding of one Hfq hexamer [P-H(I)] or two or more hexamers [P-H(II)] (Fig. 5A; see Fig. S4 in the supplemental material). The dissociation constant for each PrrF-Hfq complex was determined by fitting the fraction of bound PrrF sRNA versus the Hfq concentration to a partition function for two independent sites on PrrF (Fig. 5B). The resulting dissociation constants for P-H(I) ranged from 51 to 65 nM Hfq hexamer for PrrF1 (Table 3) and

TABLE 3 Equilibrium binding constants[a] for PrrF1, PrrF2, Hfq, and *antR*

Complex	K_{d1} (nM)	K_{d2} (nM)
PrrF1 + Hfq	65 ± 7, 51 ± 2	135 ± 12, 183 ± 407
PrrF2 + Hfq	70 ± 2, 74 ± 3	207 ± 7, 480 ± 50
antR + Hfq	295 ± 9, 302 ± 24	440 ± 500, 407 ± 943
PrrF1 + *antR*	2.5 ± 1, 7 ± 1	ND[b]

[a]Equilibrium binding constants were determined from EMSA data as described in Materials and Methods. Shown are the values ± the standard error of the fit parameter for each individual experiment (n = 2).
[b]ND, no second PrrF1-to-*antR* binding event was detected (Fig. 6A and B).

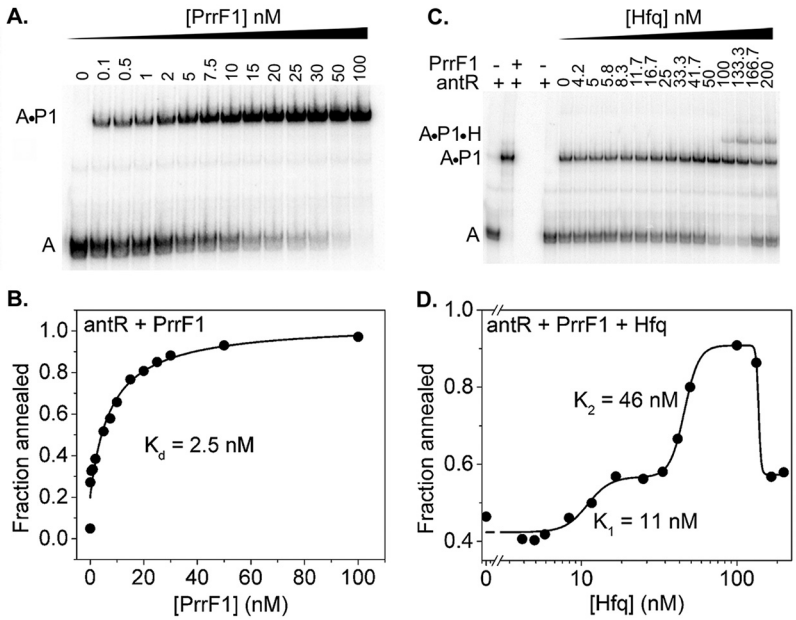

FIG 6 Effect of Hfq on sRNA-mRNA duplex stability. (A) Addition of 0 to 100 nM PrrF1 sRNA to 5 nM ^{32}P-labeled *antR* mRNA produces PrrF1-*antR* mRNA duplex. (B) A fraction of PrrF1-*antR* mRNA duplex (Fig. 5A) with increasing PrrF1 concentrations was fit to a 2-state quadratic equation (equation 3). (C) A preformed complex of 5 nM ^{32}P-*antR* mRNA and 10 nM PrrF1 sRNA was titrated with 0 to 200 nM Hfq_6 to compare the stabilities of the RNA duplex at different Hfq concentrations. An increase in the Hfq concentrations resulted in an increase of *antR*-PrrF1 (A-P1) band intensity up to 50 nM. A stable ternary complex (*antR*-PrrF1-Hfq) was visible above 50 nM Hfq_6. High Hfq concentrations destabilized the *antR*-PrrF1 duplex, resulting in free *antR* RNA. (D) The fraction of *antR* mRNA-PrrF1 complexes as a function of the Hfq concentration was fit to equation 4.

70 to 74 nM Hfq_6 for PrrF2 (Table 3; see Fig. S4 in the supplemental material). Thus, PrrF1 and PrrF2 sRNAs not only have similar sequences, they interact similarly with *P. aeruginosa* Hfq.

P. aeruginosa Hfq bound to the ^{32}P-labeled *antR* mRNA leader 4 to 6 times less tightly than to PrrF1 or PrrF2, with dissociation constants of 295 nM and 440 nM Hfq_6 for the first and second Hfq complexes, respectively (Fig. 5C and D and Table 3). This low affinity of *P. aeruginosa* Hfq for *antR* mRNA may be due to the lack of repeated $(AAN)_4$ motifs, which are necessary for efficient interaction of the distal face of Hfq with mRNAs in *E. coli* (29). In support of this idea, the short A-rich binding sequence (AAAACAGA) at the loop of SLII was only weakly protected by *P. aeruginosa* Hfq in our footprinting experiments (Fig. 4D). In contrast, many *E. coli* mRNAs contain three or four AAN triplets, which bind *E. coli* Hfq tightly (29). The weak affinity of *P. aeruginosa* Hfq for *antR* mRNA was not due to the inability of *P. aeruginosa* Hfq to recognize AAN motifs, because the K_d (dissociation constant) for *P. aeruginosa* Hfq binding to A18 RNA was 8 nM Hfq_6 (see Fig. S5 in the supplemental material), very similar to the K_d of 7.5 nM for *E. coli* Hfq (49). Moreover, *P. aeruginosa* Hfq has been reported to bind AAN repeats in *amiE* mRNA and CrcZ sRNA in *P. aeruginosa* (50, 51).

***P. aeruginosa* Hfq forms a ternary complex with PrrF1 and *antR* mRNA.** To determine whether Hfq is needed to stabilize base pairing between PrrF sRNA and *antR* mRNA, we measured the binding affinity of our *antR* mRNA fragment for PrrF1 sRNA by EMSA and found that even at 0.1 nM PrrF1, 30% of *antR* mRNA formed a complex with PrrF1 sRNA. The fraction of *antR* mRNA-PrrF1 complex as a function of the PrrF1 concentration was fit to a two-state quadratic equation, yielding a dissociation constant of 2.5 nM (Fig. 6B). Thus, PrrF1 sRNA binds tightly to *antR* mRNA in the absence of Hfq and may not require Hfq for binding to *antR* mRNA in *P. aeruginosa*.

To determine the effect of *P. aeruginosa* Hfq on the stability of the sRNA-mRNA duplex, we titrated a preformed ^{32}P-*antR* mRNA-PrrF1 complex with Hfq. Low concen-

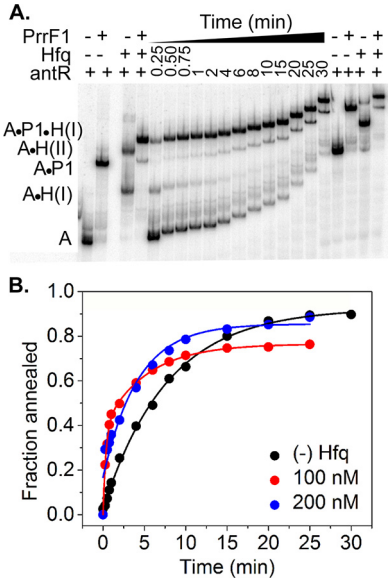

FIG 7 Effect of *P. aeruginosa* Hfq on RNA annealing kinetics. (A) 5 nM ^{32}P-*antR* RNA, 30 nM PrrF1 sRNA, and 100 nM Hfq were mixed rapidly in TNK buffer (10 mM Tris-HCl, pH 7.5, 50 mM NaCl, 50 mM KCl) and loaded on 6% native PAGE while running continuously. (B) Formation of *antR* RNA-PrrF1 binary [(−) Hfq] or the sum of *antR* RNA-PrrF1 and *antR* RNA-PrrF1-Hfq complexes (100 and 200 nM Hfq) over time were fit to a biexponential rate equation (equation 5). The controls were incubated for an hour to allow the reactions to reach equilibrium. The standard deviation among four technical replicates of each reaction was <10%.

trations of Hfq slightly increased retention of the *antR* mRNA-PrrF1 complex in the native gel. Around 50 nM Hfq, which is comparable to the dissociation constant for PrrF1 (51 nm) (Table 3), a stable ternary complex between Hfq, PrrF1, and *antR* mRNA appeared (Fig. 6D). Above 100 nM Hfq, the *antR* mRNA-PrrF1 duplexes fell apart, releasing free *antR* mRNA (Fig. 6D). This shift in the stability of the sRNA-mRNA duplex suggests that excess Hfq may sequester PrrF1 sRNA in an inactive complex that cannot pair with *antR* mRNA. A similar phenomenon was observed for *E. coli* Hfq binding to *rpoS* mRNA (52).

Hfq increases the rate of sRNA-mRNA annealing. We previously observed that *P. aeruginosa* Hfq accelerates the annealing of RNA oligomers about 10-fold (53), which is about 10-fold less than *E. coli* Hfq, a very active RNA annealer. We attribute this to replacement of an arginine (R17) with a lysine (K17) on the rim of *P. aeruginosa* Hfq (53). We next asked whether *P. aeruginosa* Hfq can also accelerate the annealing of PrrF1 sRNA with our ^{32}P-labeled *antR* mRNA fragment. Although PrrF1 bound to *antR* mRNA in the absence of Hfq, the rate of duplex formation was low (0.1 min^{-1}) (Fig. 7). In the presence of 100 nM Hfq, *antR*, PrrF1, and Hfq rapidly formed a ternary complex (k_1 = ~3 min^{-1}), which was followed by a slower phase of annealing (k_2 = 0.2 min^{-1}) and accumulation of *antR* mRNA-PrrF1 binary complex. In 200 nM Hfq, the magnitude of the fast phase was smaller, but more *antR* mRNA-PrrF1 complex accumulated within the first few minutes of the reaction than in the absence of Hfq (Fig. 7B). These data suggested that *P. aeruginosa* Hfq can increase sRNA-mRNA duplex formation by up to ~30-fold, despite weak binding of Hfq to *antR* mRNA.

DISCUSSION

The PrrF sRNAs play a central role in *P. aeruginosa* iron homeostasis and pathogenesis (14, 18, 19, 21), yet the molecular basis for Δ*prrF1,2* mutant virulence attenuation remains unclear. In this study, we aimed to determine the genetic and biochemical bases on which the PrrF sRNAs promote the production of AQs, which play multiple roles in *P. aeruginosa* virulence (24, 41, 54–56). We demonstrated that the PrrF1 and PrrF2 sRNAs redundantly affect *antR* translational activity to promote AQ production

(Fig. 2 and Table 2). We also identified two distinct regions of the *antR* leader that are required for full repression of the P_{antR}-'*lacZ* reporter *in vivo* (Fig. 3). One of these regions (mutated in the alt-*antRB* fusion) was not protected from RNase digestion in the presence of the PrrF1 sRNA (Fig. 4), suggesting these nucleotides do not directly pair with the PrrF sRNAs. Mutation of this region may instead cause structural changes to the *antR* mRNA that are important for interaction with the PrrF sRNAs, particularly since these mutations are expected to alter the stability of the stem-loop adjacent to the PrrF1 binding site. The second site identified in our *in vivo* analysis (mutated in the alt-*antRC* fusion) overlaps the *antR* translational start site (Fig. 3) and was protected from RNase digestion in the presence of PrrF1 (Fig. 4), indicating that the region pairs with the PrrF sRNAs *in vivo*. The latter region is predicted to anneal to a sequence that is completely conserved between PrrF1 and PrrF2 (Fig. 1B), providing a mechanistic rationale for the redundancy of the PrrF sRNAs in regulating *antR* expression. Notably, both the *antRA* and *antRC* mutations resulted in loss of translation under high-iron conditions, presumably due to changes in the *antR* UTR structure. In line with this idea, MFold analysis of these mutant UTRs resulted in stable hairpin structures that sequestered the Shine-Dalgarno site and translational start site of *antR* (data not shown).

Our studies also build on the current model of how *P. aeruginosa* Hfq contributes to PrrF regulation of *antR*. We showed that *P. aeruginosa* Hfq binds with high affinity to the PrrF sRNAs through the arginine patch on the Hfq rim (Fig. 4A), similar to what has been reported for several *E. coli* sRNAs (47, 48). While *P. aeruginosa* Hfq was not required for formation of the *antR*-PrrF1 complex, it increased the rate of formation of the complex and stabilized the preformed *antR*-PrrF1 complex. This biophysical evidence supports previous *in vivo* work by Sonnleitner et al., which demonstrated that a Δ*hfq* mutant was defective for PrrF-mediated regulation of *antR* (33) and that the binding potential of *P. aeruginosa* Hfq largely accounts for catabolite repression control (Crc) regulation of *antR*. Interestingly, *P. aeruginosa* Hfq bound weakly to the *antR* mRNA (295 nM) in our studies (Fig. 5D), presumably owing to a shorter A-rich motif (AAN) in contrast to the multiple AAN motifs that mediate Hfq recognition and binding to mRNAs in *E. coli* (57). This suggests either that Hfq can act via transient interactions with mRNA targets or that other RNA binding proteins contribute to mRNA recognition by *P. aeruginosa* Hfq. Nevertheless, these studies clearly demonstrate that Hfq plays an important role in PrrF-mediated regulation of *antR* expression in *P. aeruginosa*.

This study further demonstrated that iron regulates *antR* through both PrrF-dependent and PrrF-independent mechanisms (Fig. 2). This finding is consistent with previous work showing that iron activates *antA* expression in the Δ*prrF1,2* mutant (14), demonstrating that iron regulates anthranilate metabolism via AntR through at least two distinct mechanisms. In addition to serving as a precursor for AQ synthesis, anthranilate is a central metabolite in *P. aeruginosa*, and thus, its catabolism likely requires extensive control. Anthranilate is synthesized by anthranilate synthase from chorismate, which also serves as a precursor for siderophore and amino acid biosynthesis (58). Anthranilate is also formed as an intermediate in the kynurenine pathway, which converts tryptophan to NAD (NAD^+) (28, 59). Anthranilate degradation via the *antABC*-encoded anthranilate dioxygenase, which is dependent upon iron (60), feeds into the catechol ortho-cleavage pathway to form the tricarboxylic acid (TCA) cycle intermediate succinyl-coenzyme A (CoA) (61). Expression of the *antABC* operon is dependent upon the presence of anthranilate, which serves as a coinducer of the LysR-type AntR regulator (14). Thus, while PrrF regulation of *antR* expression is clearly important for AQ production in low-iron environments (Table 1) (18), many additional factors likely converge to regulate anthranilate metabolism and AQ production.

Our studies additionally identified a new TSS for the *antR* mRNA that is upstream of that observed for *P. aeruginosa* strain PA14 grown in L broth (44). Since the TSS of the longer transcript was identified under our high-iron growth conditions and not in previous studies, we hypothesize that the transcript is dependent upon iron supplementation of the growth medium. In line with this hypothesis, our data show that iron increases the activity of this upstream promoter (Fig. 2C), as well as translation of the

resulting mRNA transcript (Fig. 2B). At this time, it is unclear how iron regulates the *antR* promoter, as we did not identify an obvious Fur-binding site in the *antR-antA* intergenic region. Notably, the shorter *antR* transcript in the PA14 transcriptome lacks the Hfq binding site described here, indicating that Hfq cannot facilitate PrrF-mediated regulation of this shorter transcript. Kim and colleagues previously identified an AntR binding site immediately upstream of the TSS for the shorter *antR* transcript (62), and a potential RpoN-dependent promoter is immediately upstream of this shorter TSS (63) (shown in Fig. S1 in the supplemental material). Thus, it is possible that the shorter *antR* transcript is responsive to nitrogen and amino acid metabolism via anthranilate while the longer transcript is specifically responsive to iron. The iron-dependent transcript is additionally subject to catabolite repression control due to the ability of the CrcZ sRNA to sequester Hfq when preferred carbon sources have been depleted (33). These combined studies further demonstrate the complexity of anthranilate catabolism regulation by *P. aeruginosa* in diverse environments.

Surprisingly, our study showed disparate effects of anthranilate supplementation on C_9-PQS and C_7-PQS production by the Δ*prrF1,2* mutant (Table 1), further underlining the complexity of AQ production regulation. The alkyl chains of HHQ and C_7-PQS are derived from octanoic acid (64), and it is assumed that longer and shorter chains of different AQ congeners are derived from correspondingly longer or shorter fatty acids. We previously found that iron regulation of AQ production was variable between different congeners of each AQ metabolite (40), indicating that iron regulation of fatty acid metabolism or availability may play an important role in modulating AQ production. Combined with our current data, these studies suggest that numerous metabolic and iron-regulatory pathways modulate AQ production, highlighting the interplay of *P. aeruginosa*'s metabolic diversity, iron dependency, and pathogenic potential.

The redundancy of PrrF1 and PrrF2 observed in this work further begs the question of why the *prrF1* and *prrF2* genes are duplicated in tandem in all sequenced strains of *P. aeruginosa*. It is possible that slight differences between the PrrF1 and PrrF2 sequences allow differential regulation of some mRNA targets. Alternatively, differential expression of the PrrF1 and PrrF2 sRNAs may allow diverse environmental signals, in addition to iron depletion, to affect PrrF regulation of metabolism and virulence. Indeed, recent work by Little and colleagues demonstrated that the *P. aeruginosa* AlgZR two-component regulatory system activates PrrF expression through specific interaction with the *prrF2*, but not the *prrF1*, promoter (65). The tandem duplication of the *prrF* genes also results in the production of a longer heme response sRNA named PrrH (66). PrrH interacts with the *P. aeruginosa* Hfq protein (34), but the significance and function of this longer sRNA remain unknown. Future biophysical and genetic studies of the PrrH sRNA should yield novel insights into the physiological significance of the tandem arrangement of the *prrF* genes in *P. aeruginosa*.

MATERIALS AND METHODS

Bacterial strains and growth conditions. The strains used in these studies are summarized in Table S1 in the supplemental material. *E. coli* strains were maintained in LB medium prepared as described by Miller (67). *P. aeruginosa* strains were maintained in brain heart infusion (BHI) medium. For β-galactosidase reporter and AQ quantification studies, BHI overnight liquid cultures were inoculated from five colonies isolated on BHI agar plates. The overnight BHI cultures were diluted to an absorbance (A_{600}) of 0.05 in Chelex-treated DTSB prepared as previously described (14), with or without supplementation with 100 μM $FeCl_3$. The DTSB cultures were grown for 18 h at 37°C. Antibiotics were added at the following concentrations: for *E. coli*, ampicillin, 100 μg/ml; tetracycline, 10 or 15 μg/ml; and chloramphenicol, 12.5 μg/ml; for *P. aeruginosa*, carbenicillin, 250 μg/ml; tetracycline, 150 μg/ml.

Quantitation of AQs. AQs were quantified by LC–MS-MS as previously described (40, 41) with some modifications. Specifically, AQs were extracted from 300 μl of culture supernatants and spiked with 10 μl of 25 μM nalidixic acid as an internal standard, as previously described (6). Organic extracts were transferred to new microcentrifuge tubes and dried using a SpeedVac concentrator (Thermo-Fisher). The AQ extracts were resuspended in a mobile phase of 1:1 acetonitrile-water with 0.1% formic acid and 200 μM EDTA and separated using a dual-pump Dionex Ultimate 3000 Rapid Separation ultra-high performance liquid chromatography (UHPLC) device (Thermo-Fisher). Separation was attained using an Ascentis Express C_8 column (100 by 2.1 mm; 2.7-μm particle size; Sigma-Aldrich) maintained at 30°C. Mobile phases A and B were water with 0.1% formic acid and 200 μM EDTA, and acetonitrile with 0.1% formic acid, respectively. The mobile phase gradient was maintained at a constant flow rate of 0.4 ml/min as

follows: 20% acetonitrile for 0.5 min, followed by a linear gradient from 20% to 95% acetonitrile over 3.5 min and then 95% acetonitrile for 1.5 min. The liquid chromatography (LC) column was reequilibrated to 20% acetonitrile for 2 min between samples. LC-separated metabolites were quantified on a TSQ Quantum Ultra tandem-quadrupole mass spectrometer (Thermo-Fisher) equipped with an electrospray ionization (ESI) source in positive ion electrospray mode at a spray voltage of 3 kV maintained at 450°C. Parameters for multiple-reaction monitoring (MRM) (see Table S2 in the supplemental material) were optimized using Thermo TSQ EZ-tune software automation. Ten-point calibration curves were prepared with known concentrations of all six representative AQ species (C_7-PQS, C_9-PQS, HHQ, NHQ, HQNO, and NQNO), including a nalidixic acid standard. Unknown AQ concentrations in bacterial culture extracts were calculated by comparing the peak area ratio of a spiked internal standard to those of individual AQ species using Xcalibur version 3.0 software in Quan Browser mode (Thermo).

Determination of the *antR* transcriptional start site. The TSS of *antR* was determined using the 5′ RACE system (Invitrogen) according to the manufacturer's instructions. Briefly, total RNA was isolated from *P. aeruginosa* strain PAO1 grown in DTSB supplemented with 100 μM $FeCl_3$ for 18 h, and cDNA was synthesized by reverse transcription using a reverse primer specific to the *antR* mRNA (antR.rev) (see Table S3 in the supplemental material). After dC tailing and amplification with a nested *antR* reverse primer (antR.nested) (see Table S3 in the supplemental material), the PCR product was sequenced. The TSS of the gene was determined by looking for a series of C residues at the 5′ end of the reverse sequence. As the cDNA ends adjacent to a GGGG in the PAO1 genomic sequence, the exact TSS within this G tract is ambiguous.

Construction of *antR* reporters. The Mini-CTX1-*lacZY*$^{-SD}$ vector, which lacks the *lacZ* Shine-Dalgarno site, was constructed by PCR amplification of the *lacZY* operon, starting at the +1 translational site, from the Mini-CTX1-*lacZY* vector using the LacZ^{-SD}-HindIII-for and LacZ^{-SD}-AatI-rev primers (see Table S3 in the supplemental material). The fragment was cloned into PCR2.1 (Invitrogen), confirmed by sequencing, and then ligated into Mini-CTX1 using HindIII and AatI restriction fragments. The *antR* reporter (transcriptional and translational) (Fig. 2A) was constructed by PCR amplification of the leader and promoter sequence, spanning 67 nt upstream of the transcription start site to 15 nt downstream of the translational start site, using oligonucleotides antR(67)-EcoRI-for and antR-HindIII-rev (see Table S3 in the supplemental material) and PAO1 chromosomal DNA as the template. The PCR product was subsequently cloned into PCR2.1 and confirmed by sequencing. EcoRI-HindIII-digested fragments of the *antR* promoter and 5′ UTR were ligated into Mini-CTX1-*lacZY*$^{-SD}$ digested with the same enzymes to generate Mini-CTX1-P_{antR}-′*lacZY*$^{-SD}$. Altered *antR* reporters were generated using the QuikChange II XL site-directed mutagenesis kit (Agilent) following the manufacturer's instructions, with PCR2.1-*antR* as the template and primers alt-antR-EcoRI-for and antR-HindIII-rev (see Table S3 in the supplemental material). The *antR* translational fusion (Fig. 2B) was generated by PCR amplification of the *antR* 5′ UTR, from the +1 transcriptional site to 15 nt downstream of the translational start site, using oligonucleotides antR-UTR.for and antR-UTR.rev (see Table S3 in the supplemental material). The PCR product was subsequently cloned into PCR2.1 and confirmed by sequencing. The EcoRI-HindIII-digested fragment of the *antR* 5′ UTR was ligated into Mini-CTX-P_{lac}-*lacZY*$^{-SD}$ digested with the same enzymes to generate Mini-CTX-P_{lac}-UTR_{antR}-′*lacZY*$^{-SD}$. The *antR* transcriptional fusion was generated by PCR amplification of the *antR* promoter (from 67 nt upstream of the transcriptional start site to the transcriptional start site) using oligonucleotides antR-promoter-EcoRI-for and antR-promoter-HindIII-rev (see Table S3 in the supplemental material) and PAO1 chromosomal DNA as the template. The PCR product was subsequently cloned into PCR2.1 and confirmed by sequencing. The fragment was digested with EcoRI-HindIII and ligated into Mini-CTX1-*lacZY* digested with the same enzymes to generate the Mini-CTX1-$P_{antR'}$-*lacYZ* plasmid. All the reporter constructs were integrated at the *att* site of the PAO1, Δ*prrF1*, Δ*prrF2*, and Δ*prrF1,2* chromosomes as previously described (68).

***β*-Galactosidase activity.** β-Galactosidase activity was measured as described previously (69). Briefly, the absorbances (A_{600}) of cultures were determined, and cells were harvested by centrifugation and resuspended in potassium phosphate buffer, followed by 1:10 dilution in Z buffer. Potassium phosphate and Z buffer were prepared as previously described (69). The cells were lysed using chloroform and 0.1% sodium dodecyl sulfate (SDS). ONPG (*o*-nitrophenyl-β-D-galactopyranoside) substrate was added to the solution, and the reaction was stopped with sodium carbonate after 10 to 40 min, when a clear color change was observed. The reaction mixtures were briefly centrifuged, and the absorbance (A_{420}) of the supernatant was determined. The β-galactosidase activity was calculated in Miller units: (1,000 × A_{420})/(time [minutes] × volume [milliliters] × A_{600}).

Hfq purification. The *P. aeruginosa* Hfq protein was purified using the Impact protein purification system (NEB, Ipswitch, MA) with an N-terminal intein tag from plasmid pTYB21. Overnight cultures of Rosetta 2(DE3) cells (NEB) carrying the pTYB21 vector with the *hfq* allele, previously cloned into the multiple-cloning site (MCS) (34), were diluted 1:100 in 1 liter of LB medium containing ampicillin and chloramphenicol and grown to mid-logarithmic phase (optical density [OD], ~0.5) at 37°C with shaking. *P. aeruginosa* Hfq protein expression was then induced by addition of 1 mM IPTG (isopropyl β-D-1-thiogalactopyranoside), and cultures were grown overnight at 18°C. Cells were harvested by centrifugation at 5,000 rpm for 10 min at 4°C. The cell pellets were resuspended in 40 ml 50 mM Tris-HCl, pH 8.5, 1 M NaCl, 1 mM EDTA. The homogeneous solution was treated with 1 ml protease inhibitor cocktail (Sigma) and lysed by sonication. DNase I and RNase A were added to the sonicated solution, which was then placed on ice for 1 h. The lysates were cleared by centrifugation at 17,600 × *g* for 30 min and run through a column (10-ml bed volume) containing the chitin-binding domain (NEB; S6651). To cleave the intein tag, the column was quickly flushed with three bed volumes of cleavage buffer (50 mM Tris-HCl, pH 8.5, 1 M NaCl, 1 mM EDTA, 50 mM dithiothreitol [DTT]), column flow was stopped, and the column

was incubated overnight at 4°C. The *P. aeruginosa* Hfq protein was eluted from the column by adding an additional three bed volumes of cleavage buffer to the column. The *P. aeruginosa* Hfq protein was further cleared of nucleic acid contaminants using a cation exchange column (UNO-S6; Bio-Rad) as described previously (35). After extensive dialysis in storage buffer (50 mM Tris-HCl, pH 7.5, 250 mM NH_4Cl, 1 mM EDTA, 10% glycerol), small aliquots of *P. aeruginosa* Hfq were flash frozen and stored at −80°C. The purity of the protein was determined based on SDS-PAGE and the ratio of absorbance at 260 nm to 280 nm being less than 0.7.

RNase If footprinting. 5′-^{32}P-PrrF1 (0.1 μM) and PrrF1-Hfq complexes (8 μl) containing 0.5 μM PrrF1 and 0.17 μM to 0.67 μM *P. aeruginosa* Hfq, *E. coli* Hfq, or *E. coli* Hfq-R16A were prepared as described previously (53) and incubated for 30 min at 30°C. Samples were treated with 2 μl 1-U/μl RNase If for 1 min at 37°C, and 10 μl buffered phenol was added to stop the reaction. After extraction with phenol and chloroform and precipitation with ethanol, RNA was dissolved in 8 μl formamide loading dye (90% [vol/vol] formamide, 1× Tris-borate-EDTA [TBE], 0.1% [wt/vol] bromophenol blue, 0.1% [wt/vol] xylene cyanol) and subsequently loaded on an 8% polyacrylamide sequencing gel. Sequence ladders were obtained by nuclease digestion under denaturing conditions (70). Band intensities were integrated with SAFA (71) and normalized to bands with constant intensity in different experiments. PrrF2 samples were prepared and analyzed using the same protocol. Complexes with an *antR* mRNA fragment (nt −98 to +42 from the translational start site) were prepared as described above and treated with 2 μl 0.5-U/μl RNase If (0.75 U/μl for samples containing PrrF1) for 1 min at 37°C. Samples were processed and analyzed as described above.

Native gel mobility shift assays for PrrF sRNAs and *antR* mRNA. PrrF1 and PrrF2 sRNAs and *antR* mRNAs were transcribed *in vitro* with T7 RNA polymerase (RNAP) from a PCR template. The RNA sequences are shown in Fig. 2 and Fig. S1 in the supplemental material. Binding affinities of *P. aeruginosa* Hfq variants with ^{32}P-labeled RNAs at 30°C were measured by native gel mobility shift assays as previously described (52). The fraction of RNA in complex with one or two Hfq hexamers, R-H I or R-H II, were fit to a partition function for two nonidentical independent sites:

$$f(\text{R-HI}) = \frac{\left([\text{Hfq}]/K_{d1}\right)^n}{1 + \left(\frac{[\text{Hfq}]}{K_{d1}}\right)^n + \left(\frac{[\text{Hfq}]^2}{K_{d1}K_{d2}}\right)^n} \quad (1)$$

$$f(\text{R-HII}) = \frac{\left(\frac{[\text{Hfq}]^2}{K_{d1}K_{d2}}\right)^n}{1 + \left(\frac{[\text{Hfq}]}{K_{d1}}\right)^n + \left(\frac{[\text{Hfq}]^2}{K_{d1}K_{d2}}\right)^n} \quad (2)$$

in which K_{d1} and K_{d2} are the dissociation constants for single and multiple Hfq hexamer binding to the RNA and n is the Hill coefficient.

The equilibrium association between 5 nM ^{32}P-*antR* mRNA and unlabeled PrrF sRNAs in the absence or presence of *P. aeruginosa* Hfq was measured at 30°C as described previously (72). The fraction of *antR* mRNA-PrrF complexes as a function of the PrrF concentration was fit to a quadratic equation:

$$f(antR\text{-PrrF}) = \frac{([antR]\text{o} + [\text{PrrF}] + K_{\text{DR}}) - \sqrt{([antR]\text{o} + [\text{PrrF}] + K_{\text{DR}})^2 - 4([antR]\text{o} \times [\text{PrrF}])}}{2 \times [antR]\text{o}} \quad (3)$$

where K_{DR} is the dissociation constant for the *antR* mRNA-PrrF complex. To study the effects of Hfq on the stability of *antR* mRNA-PrrF complexes, different concentrations of *P. aeruginosa* Hfq were added to a preformed complex of 5 nM ^{32}P-*antR* mRNA and 10 nM PrrF1 and incubated at 30°C for 1 h before loading the samples on a native 6% polyacrylamide gel. The fraction of *antR* mRNA-PrrF complexes as a function of the Hfq concentration was empirically fit to a modified binding equation:

$$f(antR\text{-PrrF}) = A_0 + \frac{A_1[\text{Hfq}]^{n1}}{[\text{Hfq}]^{n1} + {K_{D1}}^{n1}} + \frac{A_2[\text{Hfq}]^{n2}}{[\text{Hfq}]^{n2} + {K_{D2}}^{n2}} - \frac{A_3[\text{Hfq}]^{n3}}{[\text{Hfq}]^{n3} + {K_{D3}}^{n3}} \quad (4)$$

in which A_0 is the fraction of *antR* mRNA-PrrF complex without Hfq; A_1, A_2, and A_3 are the changes in the fraction of *antR* mRNA-PrrF complex; and n_1, n_2, and n_3 are the Hill coefficients at different Hfq concentrations.

The association kinetics of 5 nM ^{32}P-labeled *antR* mRNA with 100 nM PrrF sRNAs in the absence or presence of Hfq was measured at 30°C by native gel mobility shift assay as described previously (52, 53, 72). The appearances of *antR* mRNA-PrrF duplex and *antR* mRNA-Hfq-sRNA ternary complex over time were fit to a pseudo-first-order biphasic rate equation:

$$f(antR - \text{PrrF}) = A_{\text{fast}}(1 - \exp(-k_{\text{fast}}t) + A_{\text{slow}}[1 - \exp(-k_{\text{slow}}t)] \quad (5)$$

SUPPLEMENTAL MATERIAL

Supplemental material for this article may be found at https://doi.org/10.1128/JB.00704-17.

SUPPLEMENTAL FILE 1, PDF file, 2.2 MB.

ACKNOWLEDGMENTS

We thank Cassandra Nelson for careful reading of the manuscript and Jace Jones for technical assistance with the mass spectrometry analysis.

This work was supported by NIH grants R01 AI123320 (to A.G.O.-S., S.A.W., and M.A.K.) and R01 GM120425 (to S.A.W.) and a University of Maryland School of Pharmacy Merit Award Fellowship (to L.D.).

REFERENCES

1. Pollack M. 1983. The role of exotoxin A in Pseudomonas disease and immunity. Rev Infect Dis 5(Suppl 5):S979–S984. https://doi.org/10.1093/clinids/5.Supplement_5.S979.
2. Vasil ML, Graham LM, Ostroff RM, Shortridge VD, Vasil AI. 1991. Phospholipase C: molecular biology and contribution to the pathogenesis of *Pseudomonas aeruginosa*. Antibiot Chemother 44:34–47. https://doi.org/10.1159/000420295.
3. Ohman DE, Burns RP, Iglewski BH. 1980. Corneal infections in mice with toxin A and elastase mutants of Pseudomonas aeruginosa. J Infect Dis 142:547–555. https://doi.org/10.1093/infdis/142.4.547.
4. Brint JM, Ohman DE. 1995. Synthesis of multiple exoproducts in *Pseudomonas aeruginosa* is under the control of RhlR-RhlI, another set of regulators in strain PAO1 with homology to the autoinducer-responsive LuxR-LuxI family. J Bacteriol 177:7155–7163. https://doi.org/10.1128/jb.177.24.7155-7163.1995.
5. Latifi A, Winson MK, Foglino M, Bycroft BW, Stewart GS, Lazdunski A, Williams P. 1995. Multiple homologues of LuxR and LuxI control expression of virulence determinants and secondary metabolites through quorum sensing in *Pseudomonas aeruginosa* PAO1. Mol Microbiol 17:333–343. https://doi.org/10.1111/j.1365-2958.1995.mmi_17020333.x.
6. Collier DN, Anderson L, McKnight SL, Noah TL, Knowles M, Boucher R, Schwab U, Gilligan P, Pesci EC. 2002. A bacterial cell to cell signal in the lungs of cystic fibrosis patients. FEMS Microbiol Lett 215:41–46. https://doi.org/10.1111/j.1574-6968.2002.tb11367.x.
7. Minandri F, Imperi F, Frangipani E, Bonchi C, Visaggio D, Facchini M, Pasquali P, Bragonzi A, Visca P. 2016. Role of iron uptake systems in *Pseudomonas aeruginosa* virulence and airway infection. Infect Immun 84:2324–2335. https://doi.org/10.1128/IAI.00098-16.
8. Hood MI, Skaar EP. 2012. Nutritional immunity: transition metals at the pathogen-host interface. Nat Rev Microbiol 10:525–537. https://doi.org/10.1038/nrmicro2836.
9. Meyer JM, Neely A, Stintzi A, Georges C, Holder IA. 1996. Pyoverdine is essential for virulence of *Pseudomonas aeruginosa*. Infect Immun 64:518–523.
10. Takase H, Nitanai H, Hoshino K, Otani T. 2000. Requirement of the *Pseudomonas aeruginosa tonB* gene for high-affinity iron acquisition and infection. Infect Immun 68:4498–4504. https://doi.org/10.1128/IAI.68.8.4498-4504.2000.
11. Takase H, Nitanai H, Hoshino K, Otani T. 2000. Impact of siderophore production on *Pseudomonas aeruginosa* infections in immunosuppressed mice. Infect Immun 68:1834–1839. https://doi.org/10.1128/IAI.68.4.1834-1839.2000.
12. Reinhart AA, Oglesby-Sherrouse AG. 2016. Regulation of *Pseudomonas aeruginosa* virulence by distinct iron sources. Genes (Basel) 7:E126. https://doi.org/10.3390/genes7120126.
13. Wiens JR, Vasil AI, Schurr MJ, Vasil ML. 2014. Iron-regulated expression of alginate production, mucoid phenotype, and biofilm formation by *Pseudomonas aeruginosa*. mBio 5:e01010-01013. https://doi.org/10.1128/mBio.01010-13.
14. Oglesby AG, Farrow JM III, Lee JH, Tomaras AP, Greenberg EP, Pesci EC, Vasil ML. 2008. The influence of iron on *Pseudomonas aeruginosa* physiology: a regulatory link between iron and quorum sensing. J Biol Chem 283:15558–15567. https://doi.org/10.1074/jbc.M707840200.
15. Banin E, Vasil ML, Greenberg EP. 2005. Iron and *Pseudomonas aeruginosa* biofilm formation. Proc Natl Acad Sci U S A 102:11076–11081. https://doi.org/10.1073/pnas.0504266102.
16. Lamont IL, Beare PA, Ochsner U, Vasil AI, Vasil ML. 2002. Siderophore-mediated signaling regulates virulence factor production in *Pseudomonas aeruginosa*. Proc Natl Acad Sci U S A 99:7072–7077. https://doi.org/10.1073/pnas.092016999.
17. Wilderman PJ, Vasil AI, Johnson Z, Wilson MJ, Cunliffe HE, Lamont IL, Vasil ML. 2001. Characterization of an endoprotease (PrpL) encoded by a PvdS-regulated gene in *Pseudomonas aeruginosa*. Infect Immun 69:5385–5394.
18. Reinhart AA, Nguyen AT, Brewer LK, Bevere J, Jones JW, Kane MA, Damron FH, Barbier M, Oglesby-Sherrouse AG. 2017. The *Pseudomonas aeruginosa* PrrF small RNAs regulate iron homeostasis during acute murine lung infection. Infect Immun 85:e00764-16. https://doi.org/10.1128/IAI.00764-16.
19. Reinhart AA, Powell DA, Nguyen AT, O'Neill M, Djapgne L, Wilks A, Ernst RK, Oglesby-Sherrouse AG. 2015. The *prrF*-encoded small regulatory RNAs are required for iron homeostasis and virulence of *Pseudomonas aeruginosa*. Infect Immun 83:863–875. https://doi.org/10.1128/IAI.02707-14.
20. Winsor GL, Griffiths EJ, Lo R, Dhillon BK, Shay JA, Brinkman FS. 2016. Enhanced annotations and features for comparing thousands of Pseudomonas genomes in the Pseudomonas genome database. Nucleic Acids Res 44:D646–D653. https://doi.org/10.1093/nar/gkv1227.
21. Wilderman PJ, Sowa NA, FitzGerald DJ, FitzGerald PC, Gottesman S, Ochsner UA, Vasil ML. 2004. Identification of tandem duplicate regulatory small RNAs in *Pseudomonas aeruginosa* involved in iron homeostasis. Proc Natl Acad Sci U S A 101:9792–9797. https://doi.org/10.1073/pnas.0403423101.
22. Kim K, Kim YU, Koh BH, Hwang SS, Kim SH, Lepine F, Cho YH, Lee GR. 2010. HHQ and PQS, two *Pseudomonas aeruginosa* quorum-sensing molecules, down-regulate the innate immune responses through the nuclear factor-kappaB pathway. Immunology 129:578–588. https://doi.org/10.1111/j.1365-2567.2009.03160.x.
23. Deziel E, Lepine F, Milot S, He J, Mindrinos MN, Tompkins RG, Rahme LG. 2004. Analysis of Pseudomonas aeruginosa 4-hydroxy-2-alkylquinolines (HAQs) reveals a role for 4-hydroxy-2-heptylquinoline in cell-to-cell communication. Proc Natl Acad Sci U S A 101:1339–1344. https://doi.org/10.1073/pnas.0307694100.
24. Calfee MW, Coleman JP, Pesci EC. 2001. Interference with *Pseudomonas* quinolone signal synthesis inhibits virulence factor expression by *Pseudomonas aeruginosa*. Proc Natl Acad Sci U S A 98:11633–11637. https://doi.org/10.1073/pnas.201328498.
25. Lemma E, Simon J, Schagger H, Kroger A. 1995. Properties of the menaquinol oxidase (Qox) and of *qox* deletion mutants of *Bacillus subtilis*. Arch Microbiol 163:432–438. https://doi.org/10.1007/BF00272132.
26. Tynecka Z, Malm A. 1985. The effect of DCCD, HQNO or Cd2+ on glutamate oxidation in *Staphylococcus aureus*. Ann Univ Mariae Curie Sklodowska Med 40:149–155.
27. Van Ark G, Berden JA. 1977. Binding of HQNO to beef-heart submitochondrial particles. Biochim Biophys Acta 459:119–127. https://doi.org/10.1016/0005-2728(77)90014-7.
28. Farrow JM III, Pesci EC. 2007. Two distinct pathways supply anthranilate as a precursor of the *Pseudomonas* quinolone signal. J Bacteriol 189:3425–3433. https://doi.org/10.1128/JB.00209-07.
29. Soper T, Mandin P, Majdalani N, Gottesman S, Woodson SA. 2010. Positive regulation by small RNAs and the role of Hfq. Proc Natl Acad Sci U S A 107:9602–9607. https://doi.org/10.1073/pnas.1004435107.
30. Dimastrogiovanni D, Frohlich KS, Bandyra KJ, Bruce HA, Hohensee S, Vogel J, Luisi BF. 2014. Recognition of the small regulatory RNA RydC by the bacterial Hfq protein. Elife 2014:3. https://doi.org/10.7554/eLife.05375.
31. Gottesman S, McCullen CA, Guillier M, Vanderpool CK, Majdalani N, Benhammou J, Thompson KM, FitzGerald PC, Sowa NA, FitzGerald DJ. 2006. Small RNA regulators and the bacterial response to stress. Cold Spring Harbor Symp Quant Biol 71:1–11. https://doi.org/10.1101/sqb.2006.71.016.
32. Masse E, Escorcia FE, Gottesman S. 2003. Coupled degradation of a small regulatory RNA and its mRNA targets in *Escherichia coli*. Genes Dev 17:2374–2383. https://doi.org/10.1101/gad.1127103.
33. Sonnleitner E, Prindl K, Blasi U. 2017. The Pseudomonas aeruginosa CrcZ RNA interferes with Hfq-mediated riboregulation. PLoS One 12:e0180887. https://doi.org/10.1371/journal.pone.0180887.
34. Osborne J, Djapgne L, Tran BQ, Goo YA, Oglesby-Sherrouse AG. 2014. A method for *in vivo* identification of bacterial small RNA-binding proteins. Microbiologyopen 3:950–960. https://doi.org/10.1002/mbo3.220.
35. Peng Y, Soper TJ, Woodson SA. 2014. Positional effects of AAN motifs in

rpoS regulation by sRNAs and Hfq. J Mol Biol 426:275–285. https://doi.org/10.1016/j.jmb.2013.08.026.
36. Panja S, Schu DJ, Woodson SA. 2013. Conserved arginines on the rim of Hfq catalyze base pair formation and exchange. Nucleic Acids Res 41:7536–7546. https://doi.org/10.1093/nar/gkt521.
37. Nielsen JS, Lei LK, Ebersbach T, Olsen AS, Klitgaard JK, Valentin-Hansen P, Kallipolitis BH. 2010. Defining a role for Hfq in Gram-positive bacteria: evidence for Hfq-dependent antisense regulation in *Listeria monocytogenes*. Nucleic Acids Res 38:907–919. https://doi.org/10.1093/nar/gkp1081.
38. Metruccio MM, Fantappie L, Serruto D, Muzzi A, Roncarati D, Donati C, Scarlato V, Delany I. 2009. The Hfq-dependent small noncoding RNA NrrF directly mediates Fur-dependent positive regulation of succinate dehydrogenase in *Neisseria meningitidis*. J Bacteriol 191:1330–1342. https://doi.org/10.1128/JB.00849-08.
39. Papenfort K, Said N, Welsink T, Lucchini S, Hinton JC, Vogel J. 2009. Specific and pleiotropic patterns of mRNA regulation by ArcZ, a conserved, Hfq-dependent small RNA. Mol Microbiol 74:139–158. https://doi.org/10.1111/j.1365-2958.2009.06857.x.
40. Nguyen AT, Jones JW, Camara M, Williams P, Kane MA, Oglesby-Sherrouse AG. 2016. Cystic fibrosis isolates of *Pseudomonas aeruginosa* retain iron-regulated antimicrobial activity against *Staphylococcus aureus* through the action of multiple alkylquinolones. Front Microbiol 7:1171–1183. https://doi.org/10.3389/fmicb.2016.01171.
41. Nguyen AT, Jones JW, Ruge MA, Kane MA, Oglesby-Sherrouse AG. 2015. Iron depletion enhances production of antimicrobials by *Pseudomonas aeruginosa*. J Bacteriol 197:2265–2275. https://doi.org/10.1128/JB.00072-15.
42. Nguyen AT, O'Neill MJ, Watts AM, Robson CL, Lamont IL, Wilks A, Oglesby-Sherrouse AG. 2014. Adaptation of iron homeostasis pathways by a *Pseudomonas aeruginosa* pyoverdine mutant in the cystic fibrosis lung. J Bacteriol 196:2265–2276. https://doi.org/10.1128/JB.01491-14.
43. Lepine F, Milot S, Deziel E, He J, Rahme LG. 2004. Electrospray/mass spectrometric identification and analysis of 4-hydroxy-2-alkylquinolines (HAQs) produced by Pseudomonas aeruginosa. J Am Soc Mass Spectrom 15:862–869. https://doi.org/10.1016/j.jasms.2004.02.012.
44. Wurtzel O, Yoder-Himes DR, Han K, Dandekar AA, Edelheit S, Greenberg EP, Sorek R, Lory S. 2012. The single-nucleotide resolution transcriptome of Pseudomonas aeruginosa grown in body temperature. PLoS Pathog 8:e1002945. https://doi.org/10.1371/journal.ppat.1002945.
45. Morita T, Nishino R, Aiba H. 2017. Role of the terminator hairpin in the biogenesis of functional Hfq-binding sRNAs. RNA 23:1419–1431. https://doi.org/10.1261/rna.060756.117.
46. Sauer E, Weichenrieder O. 2011. Structural basis for RNA 3′-end recognition by Hfq. Proc Natl Acad Sci U S A 108:13065–13070. https://doi.org/10.1073/pnas.1103420108.
47. Sauer E, Schmidt S, Weichenrieder O. 2012. Small RNA binding to the lateral surface of Hfq hexamers and structural rearrangements upon mRNA target recognition. Proc Natl Acad Sci U S A 109:9396–9401. https://doi.org/10.1073/pnas.1202521109.
48. Zhang A, Schu DJ, Tjaden BC, Storz G, Gottesman S. 2013. Mutations in interaction surfaces differentially impact E. coli Hfq association with small RNAs and their mRNA targets. J Mol Biol 425:3678–3697. https://doi.org/10.1016/j.jmb.2013.01.006.
49. Santiago-Frangos A, Kavita K, Schu DJ, Gottesman S, Woodson SA. 2016. C-terminal domain of the RNA chaperone Hfq drives sRNA competition and release of target RNA. Proc Natl Acad Sci U S A 113:E6089–E6096. https://doi.org/10.1073/pnas.1613053113.
50. Sonnleitner E, Blasi U. 2014. Regulation of Hfq by the RNA CrcZ in Pseudomonas aeruginosa carbon catabolite repression. PLoS Genet 10:e1004440. https://doi.org/10.1371/journal.pgen.1004440.
51. Sonnleitner E, Abdou L, Haas D. 2009. Small RNA as global regulator of carbon catabolite repression in Pseudomonas aeruginosa. Proc Natl Acad Sci U S A 106:21866–21871. https://doi.org/10.1073/pnas.0910308106.
52. Lease RA, Woodson SA. 2004. Cycling of the Sm-like protein Hfq on the DsrA small regulatory RNA. J Mol Biol 344:1211–1223. https://doi.org/10.1016/j.jmb.2004.10.006.
53. Zheng A, Panja S, Woodson SA. 2016. Arginine patch predicts the RNA annealing activity of Hfq from Gram-negative and Gram-positive bacteria. J Mol Biol 428:2259–2264. https://doi.org/10.1016/j.jmb.2016.03.027.
54. Filkins LM, Graber JA, Olson DG, Dolben EL, Lynd LR, Bhuju S, O'Toole GA. 2015. Coculture of *Staphylococcus aureus* with *Pseudomonas aeruginosa* drives *S. aureus* towards fermentative metabolism and reduced viability in a cystic fibrosis model. J Bacteriol 197:2252–2264. https://doi.org/10.1128/JB.00059-15.
55. Korgaonkar A, Trivedi U, Rumbaugh KP, Whiteley M. 2013. Community surveillance enhances *Pseudomonas aeruginosa* virulence during polymicrobial infection. Proc Natl Acad Sci U S A 110:1059–1064. https://doi.org/10.1073/pnas.1214550110.
56. Hazan R, Que YA, Maura D, Strobel B, Majcherczyk PA, Hopper LR, Wilbur DJ, Hreha TN, Barquera B, Rahme LG. 2016. Auto poisoning of the respiratory chain by a quorum-sensing-regulated molecule favors biofilm formation and antibiotic tolerance. Curr Biol 26:195–206. https://doi.org/10.1016/j.cub.2015.11.056.
57. Peng Y, Curtis JE, Fang X, Woodson SA. 2014. Structural model of an mRNA in complex with the bacterial chaperone Hfq. Proc Natl Acad Sci U S A 111:17134–17139. https://doi.org/10.1073/pnas.1410114111.
58. Herrmann KM, Weaver LM. 1999. The shikimate pathway. Annu Rev Plant Physiol Plant Mol Biol 50:473–503. https://doi.org/10.1146/annurev.arplant.50.1.473.
59. Palmer GC, Jorth PA, Whiteley M. 2013. The role of two *Pseudomonas aeruginosa* anthranilate synthases in tryptophan and quorum signal production. Microbiology 159:959–969. https://doi.org/10.1099/mic.0.063065-0.
60. Eby DM, Beharry ZM, Coulter ED, Kurtz DM, Jr, Neidle EL. 2001. Characterization and evolution of anthranilate 1,2-dioxygenase from Acinetobacter sp. strain ADP1. J Bacteriol 183:109–118. https://doi.org/10.1128/JB.183-1.109-118.2001.
61. Urata M, Miyakoshi M, Kai S, Maeda K, Habe H, Omori T, Yamane H, Nojiri H. 2004. Transcriptional regulation of the *ant* operon, encoding two-component anthranilate 1,2-dioxygenase, on the carbazole-degradative plasmid pCAR1 of *Pseudomonas resinovorans* strain CA10. J Bacteriol 186:6815–6823. https://doi.org/10.1128/JB.186.20.6815-6823.2004.
62. Kim SK, Im SJ, Yeom DH, Lee JH. 2012. AntR-mediated bidirectional activation of *antA* and *antR*, anthranilate degradative genes in *Pseudomonas aeruginosa*. Gene 505:146–152. https://doi.org/10.1016/j.gene.2012.05.004.
63. Miyakoshi M, Shintani M, Terabayashi T, Kai S, Yamane H, Nojiri H. 2007. Transcriptome analysis of Pseudomonas putida KT2440 harboring the completely sequenced IncP-7 plasmid pCAR1. J Bacteriol 189:6849–6860. https://doi.org/10.1128/JB.00684-07.
64. Dulcey CE, Dekimpe V, Fauvelle DA, Milot S, Groleau MC, Doucet N, Rahme LG, Lepine F, Deziel E. 2013. The end of an old hypothesis: the pseudomonas signaling molecules 4-hydroxy-2-alkylquinolines derive from fatty acids, not 3-ketofatty acids. Chem Biol 20:1481–1491. https://doi.org/10.1016/j.chembiol.2013.09.021.
65. Little AS, Okkotsu Y, Reinhart AA, Damron FH, Barbier M, Barrett B, Oglesby-Sherrouse AG, Goldberg JB, Cody WL, Schurr MJ, Vasil ML, Schurr MJ. 2018. Pseudomonas aeruginosa AlgR phosphorylation status differentially regulates pyocyanin and pyoverdine production. mBio 30:e02318-17. https://doi.org/10.1128/mBio.02318-17.
66. Oglesby-Sherrouse AG, Vasil ML. 2010. Characterization of a heme-regulated non-coding RNA encoded by the *prrF* locus of *Pseudomonas aeruginosa*. PLoS One 5:e9930. https://doi.org/10.1371/journal.pone.0009930.
67. Miller JH. 1972. Experiments in molecular genetics. Cold Spring Harbor Laboratory, Cold Spring Harbor, NY.
68. Hoang TT, Kutchma AJ, Becher A, Schweizer HP. 2000. Integration-proficient plasmids for *Pseudomonas aeruginosa*: site-specific integration and use for engineering of reporter and expression strains. Plasmid 43:59–72. https://doi.org/10.1006/plas.1999.1441.
69. Sambrook J, Russell DW. 2001. Molecular cloning: a laboratory manual, 3rd ed. Cold Spring Harbor Laboratory Press, Cold Spring Harbor, NY.
70. Donis-Keller H, Maxam AM, Gilbert W. 1977. Mapping adenines, guanines, and pyrimidines in RNA. Nucleic Acids Res 4:2527–2538. https://doi.org/10.1093/nar/4.8.2527.
71. Das R, Laederach A, Pearlman SM, Herschlag D, Altman RB. 2005. SAFA: semi-automated footprinting analysis software for high-throughput quantification of nucleic acid footprinting experiments. RNA 11:344–354. https://doi.org/10.1261/rna.7214405.
72. Soper TJ, Woodson SA. 2008. The rpoS mRNA leader recruits Hfq to facilitate annealing with DsrA sRNA. RNA 14:1907–1917. https://doi.org/10.1261/rna.1110608.
73. Zuker M. 2003. Mfold Web server for nucleic acid folding and hybridization prediction. Nucleic Acids Res 31:3406–3415. https://doi.org/10.1093/nar/gkg595.